JOURNAL OF MATERIALS SCIENCE **36** (2001) 503–510

9 MeV Au ion implantation into Ti and Ti-6Al-4V

R. TREJO-LUNA, L. R. DE LA VEGA, J. RICKARDS
Instituto de Física, Universidad Nacional Autónoma de México, Ap. Postal 20-364, México, D.F. 01000, Mexico
E-mail: rickards@fenix.ifisicacu.unum.mx

C. FALCONY
Departamento de Física, CINVESTAV, Instituto Politécnico Nacional, Ap. Postal 14-740, México, D.F. 07000, México

M. JERGEL
Institute of Physics, Slovak Academy of Sciences, Dubravskka cesta 9, 842 28 Bratislava, Slovakia

Titanium and Ti-6Al-4V alloy samples were implanted with 9 MeV Au ions at room temperature with fluences up to 6.5×10^{20} ions/m^2. The results were analyzed using Rutherford backscattering, X-ray diffraction, glancing angle X-ray diffraction, and SEM. The glancing angle diffraction patterns show peaks corresponding to a new phase in both materials, presenting an hcp structure with larger lattice parameters than the unimplanted material. This phase is formed mainly by structural damage produced by the beam, and not by the formation of compounds. Modifications of the grain size and microstrain were measured using the Williamson-Hall method.

1. Introduction

Titanium and its alloys are some of the best currently available materials for surgical implants. They present excellent corrosion resistance and biocompatibility, good ductility, low elastic modulus and low density. In particular, the alloy Ti-6Al-4V has high tensile strength and fatigue resistance [1–4]. At room temperature, pure titanium is normally found in the α phase, which is a hcp structure. Above 1155 K there is a transformation to the bcc β phase, and at high pressures it transforms to a simple hexagonal ω phase. The ω phase has also been reported as a result of high energy ion irradiation [5, 6].

Ion implantation has numerous advantages for treating biomaterial surfaces. One is the selective surface modification without affecting bulk properties; another is the possibility of performing the process at low temperatures. It is known that implantation of certain types of ions into titanium hardens the surface, reduces friction, and improves the wear resistance. The hardening is attributed primarily to the formation of hard phase (carbide, nitride and oxide) precipitates [4].

As part of a program to improve the surface properties of Ti and its alloys for medical applications, and to understand the mechanisms involved in these changes, here we present the results of 9 MeV Au ion implantation into Ti and the alloy Ti-6Al-4V. At this beam energy, the implanted ions affect the first 1.5 μm below the surface of the metal. The relatively low sputtering yield reduces the surface damage which is normally present in low energy implantations, so it is possible to study the final distribution of implanted species and structural damage, unhindered by surface removal effects. Most previous studies of ion implantation into titanium have been made at low energies, and studies have been made of very high energy ion irradiation of Ti, leading to a phase transformation [5, 6].

2. Experiment

The Ti samples were 99.6% purity, the main impurities quoted by the manufacturer (Goodfellow) being Al, Cr, Mn, Ni, and V at 500 ppm. They consisted of slices cut from 9.5 mm diameter rods which were annealed in argon at 675°C by the manufacturer. After cutting, they were polished with Emery paper and 0.05 μm alumina. Titanium normally has a hcp crystal structure with lattice parameters $a = 0.2950$ nm and $c = 0.4686$ nm [7]; this was verified by x-ray diffraction on untreated samples in the present experiment. For the unimplanted samples, metallographic and SEM images in the present experiment show a large-grain structure with an average size of the order of 100 μm. Small angle x-ray diffraction measurements indicated an additional mosaic structure with sizes of 56 nm at 1 μm depth, obtained with the Williamson-Hall method described later.

The Ti-6Al-4V alloy samples were similarly cut from 10.0 mm diameter rods, also purchased from Goodfellow, and polished with Emery paper and 0.05 μm alumina. The maximum impurity quoted by the manufacturer is 650 ppm of oxygen. Scanning electron microprobe and x- ray diffraction measurements were carried out on untreated samples, showing 10–15 μm

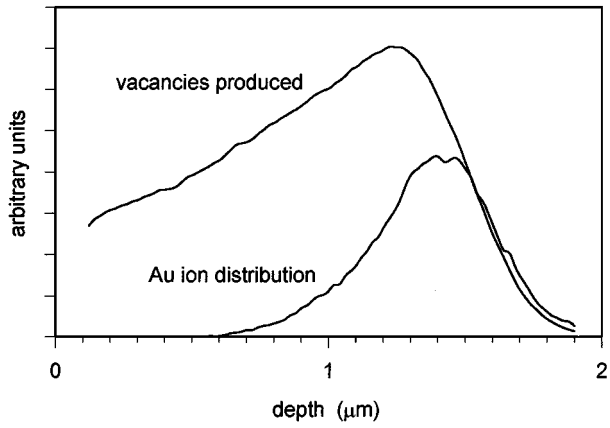

Figure 1 Calculations of final Au ion distribution and vacancy distribution, for 9 MeV Au ions striking a Ti target.

diameter, V-depleted α phase grains (hcp with $a = 0.2925$ nm and $c = 0.4670$ nm) in a V-enriched β phase matrix (bcc with $a = 0.3230$ nm) which surrounds the α phase grains. These values are in agreement with the literature [8]. The size of the mosaic structure at 1 μm depth was determined with the Williamson-Hall plot to be 71 nm.

The 9 MeV Au ion (3^+) implantation was performed at room temperature using the Instituto de Física 3 MV 9SDH-2 Pelletron accelerator. Typical target currents were 1 to 3 μA, and the beam was rastered over 4 cm^2, with which flux densities of 0.5 to 1.5×10^{16} Au ions/m^{2}s were obtained. Various fluences were studied, the maximum fluence being 6.5×10^{20} Au ions/m^2. According to TRIM [9] calculations, the projected range of 9 MeV Au ions in Ti is 1.37 μm, with a straggling of 0.22 μm. The same calculation indicates that a fluence of 10^{20} Au ions/m^2 corresponds to 0.35 atomic % in the peak of the implanted Au ion distribution.

Although the final Au ion distribution is calculated to be a slightly skewed Gaussian, damage occurs all along the ion trajectory, as shown in Fig. 1, which is a smoothed calculation of the vacancy distribution and the final ion distribution, using TRIM, with arbitrary vertical scales. A measure of the amount of structural damage produced by nuclear stopping is the average number of displacements each atom of the material suffers during the total bombardment. For a fluence of 10^{20} Au ions/m^2, the number displacements per atom (dpa) was calculated to be above 30 in the peak of the vacancy distribution at a depth of about 1.2 μm. The calculations corresponding to the Ti-6Al-4V alloy yield very similar results.

Conventional (XRD) and grazing angle x-ray diffraction (GXRD) were used to analyze the samples. The grazing angle measurements were performed on a Siemens D5000 diffractometer with a grazing incidence attachment and LiF crystal monochromator in the secondary beam path, using the CuKα radiation. The diffraction patterns were taken with the sample fixed at the angles of incidence $\alpha = 0.5^\circ$, 1°, 1.5°, 2°, 2.5°, and 3°, and with a scintillation detector moving from $2\theta = 30^\circ$ to 80° with a step of 0.02° at each angle of incidence. The collection time at each value of 2θ was 5s. Here θ is the diffraction angle. The angle of incidence 0.5° is slightly above the critical angle for total external reflection, when the x-rays start to penetrate the material; by increasing this angle the penetration depth is gradually increased. For example, at $\alpha = 1^\circ$, 90% of the scattered intensity comes from a depth smaller than ≈ 1 μm.

3. Results

Using the same Pelletron accelerator, the backscattering (RBS) of ^{4}He ions was performed in order to determine the final position of the implanted Au ions. In this technique [10], the measured energy spectrum of the backscattered He ions is used to determine the depth of the Au ions below the surface of the sample. Conventionally, RBS measurements are done with 2 MeV He ions, but in the present case at 2 MeV the Au peak in the RBS spectrum was hidden beneath the continuum due to the thick Ti. Therefore it was necessary to raise the He ion energy to 6 MeV at which energy the signal from the Au implants was separated from that of the solid Ti in the spectra. Fig. 2 shows a spectrum of backscattered ^{4}He on Ti implanted with 10^{20} Au ions/m^2. The RBS spectrum from the Ti-6Al-4V alloy was essentially the same. The measured profile of the Au implant turned out to be approximately Gaussian; it was fit with the code RUMP [11] with a Gaussian distribution with a mean depth of 1.50 μm and a FWHM of 0.62 μm. The measured mean depth is in reasonable agreement with the calculated value (1.37 μm), but the measured width is about 2.5 times greater than the calculated one (0.22 μm).

When ion implantation is performed at lower energies (100–200 keV), there is frequently a combination of a small ion range and a large sputtering yield. This leads to a modification of the implanted species depth profile, as the eroded surface recedes as much as, or even more than the initial ion range. It also places a limit on the number of ions that can be implanted, since initially implanted ions may be sputtered away at a later stage. In the present experiment, all the spectra obtained from RBS similar to Fig. 2 indicate that

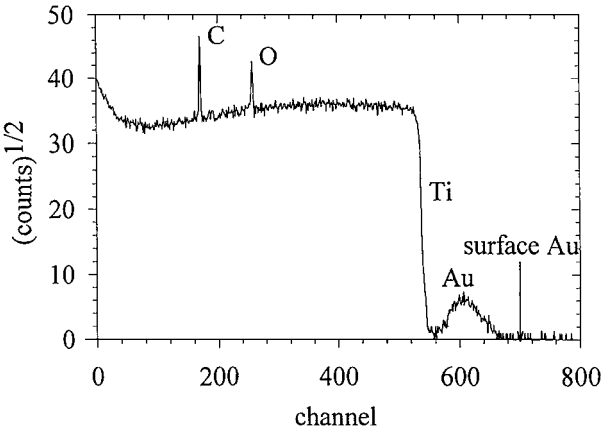

Figure 2 RBS spectrum of 6 MeV alpha particles scattered from titanium implanted with 9 MeV Au ions. The implanted Au ions are found at a mean depth of 1.50 μm with a FWHM of 0.62 μm. The arrow indicates the position where the Au peak would appear if it were on the surface. There is a carbon contamination and a thin oxygen surface peak.

this effect does not occur, for the Gaussian distribution is well defined, and it appears at the correct depth. This is consistent with a small sputtering coefficient, which for the present case of 9 MeV Au on Ti, was calculated with TRIM to be between 2 and 3.

The measured width of the implanted Au distribution is larger than expected from the calculations. This could be due to diffusion arising from local heating of the material during bombardment. However, it will be seen that radiation damage during the implantation caused considerable changes in the crystal structure and grain sizes, so the accompanying strain could very well account for the observed increase in width.

The microstructure of both Ti and the Ti-6Al-4V alloy before implantation, was revealed with a solution of 10% HF, 5% HNO_3 and 85% H_2O, and then the samples were observed with SEM and optical microscopy. Fig. 3 shows the surface of unimplanted Ti, where the microstructure corresponds to α–Ti and presents a large grain size ($\sim$100 μm). The dark and light grains are both α; the contrast is caused by the dependence of the etching effect on the orientation of the crystal [12].

Fig. 4 is the corresponding image of unimplanted Ti-6Al-4V. The microstructure in this case consists of two phases, α and β; the dark regions correspond to the α phase, and the light regions to the β phase surrounding the α phase regions [13]. An electron microprobe study showed the α phase to be depleted in V, while the β phase is rich in V.

The Au ion implantation process revealed the microstructure on the surface of both metals, so it was not necessary to chemically etch the samples in order to view the grain structure. In the case of Ti (Fig. 5), the boundaries of the large grains were strongly revealed with a fluence of 6.5×10^{20} Au ions/m^2, and an accumulation of matter at the boundaries is evident. In addition, on the surface of the grains, new parallel structures were revealed, suggesting twinning. In the Ti-6Al-4V case there is no evident change in the microstructure for 6.5×10^{20} Au ions/m^2, compared with the unimplanted samples.

Vickers microhardness tests (10 grams load for 20 seconds) were performed on reference samples and on samples implanted with different fluences of Au ions. The results are shown in Fig. 6. In the case of Ti, an increase of 75% in hardness is observed for a fluence of 10^{20} Au ions/m^2 and then a slight decrease. For the Ti-6Al-4V alloy the increase is up to 100% for 10^{20} Au ions/m^2 and continues to increase for a higher fluence.

3.1. Titanium

XRD and GXRD patterns were taken from samples of Ti and the Ti-6Al-4V alloy, both in reference samples and in samples implanted with different values of Au ion fluence. Although it is known that there is always a thin oxide present on Ti and alloy surfaces, no oxide lines were observed in these patterns, indicating that the oxide is very thin. The hexagonal close packed (hcp) polycrystalline structure of Ti was confirmed in the reference samples by the presence of all the tabulated diffraction maxima [14]. The same was true of those implanted with 10^{18} and 10^{19} Au ions/m^2. For all

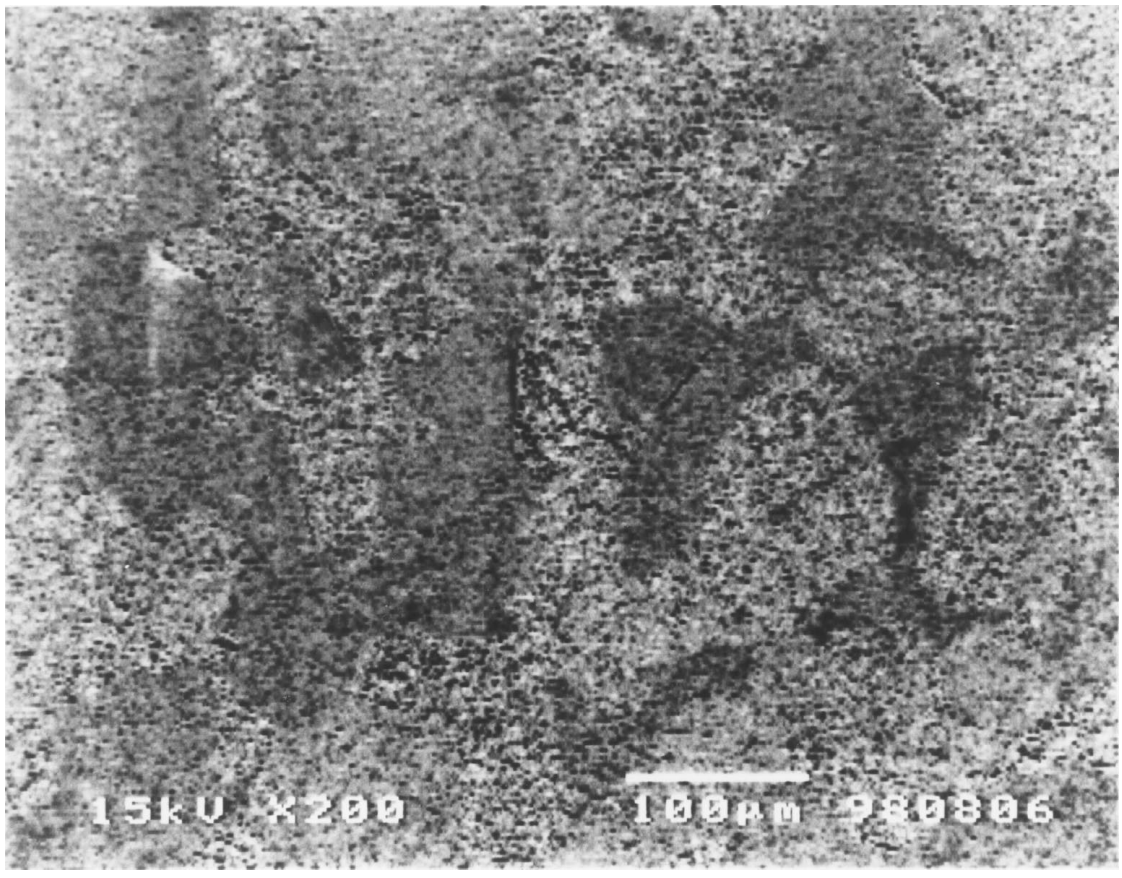

Figure 3 SEM micrograph of reference Ti, showing the large grain structure in the original material, revealed by chemical etching.

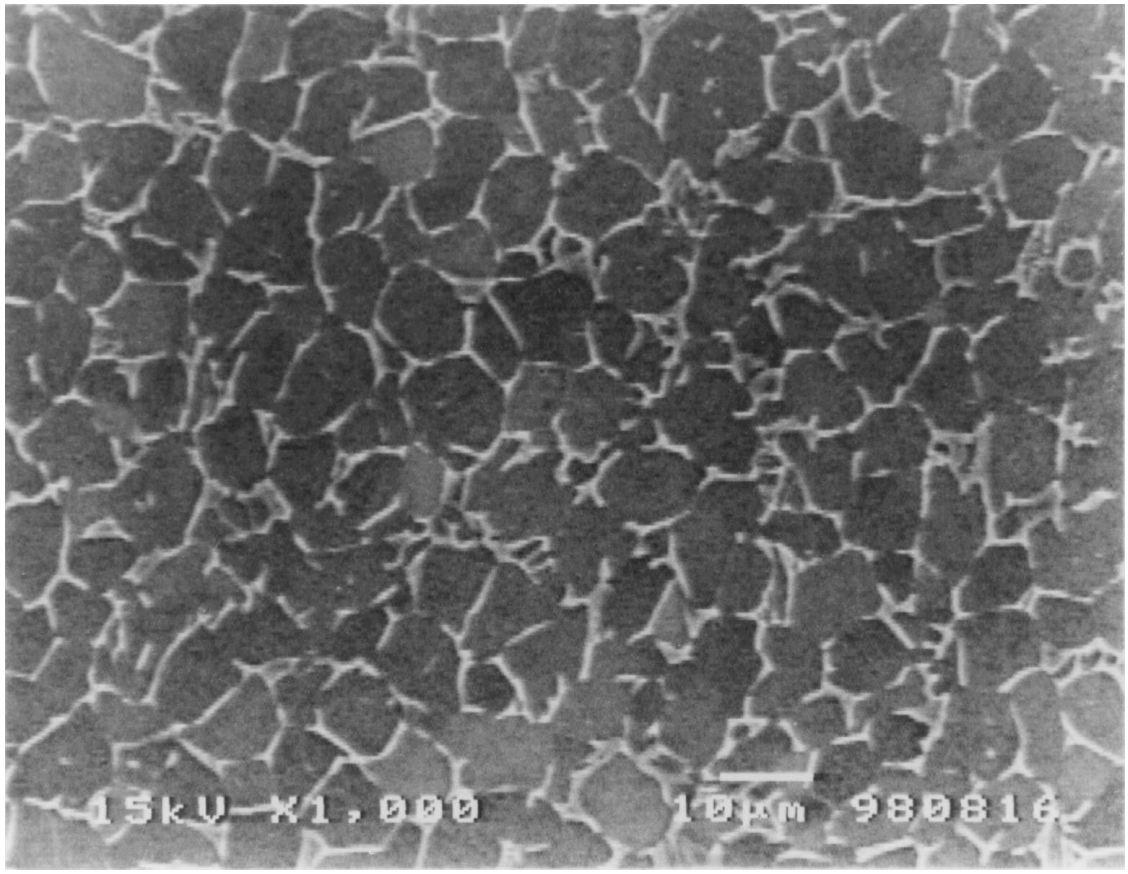

Figure 4 SEM micrograph of reference Ti-6Al-4V, showing the α (dark) and β (light) phases, revealed by chemical etching.

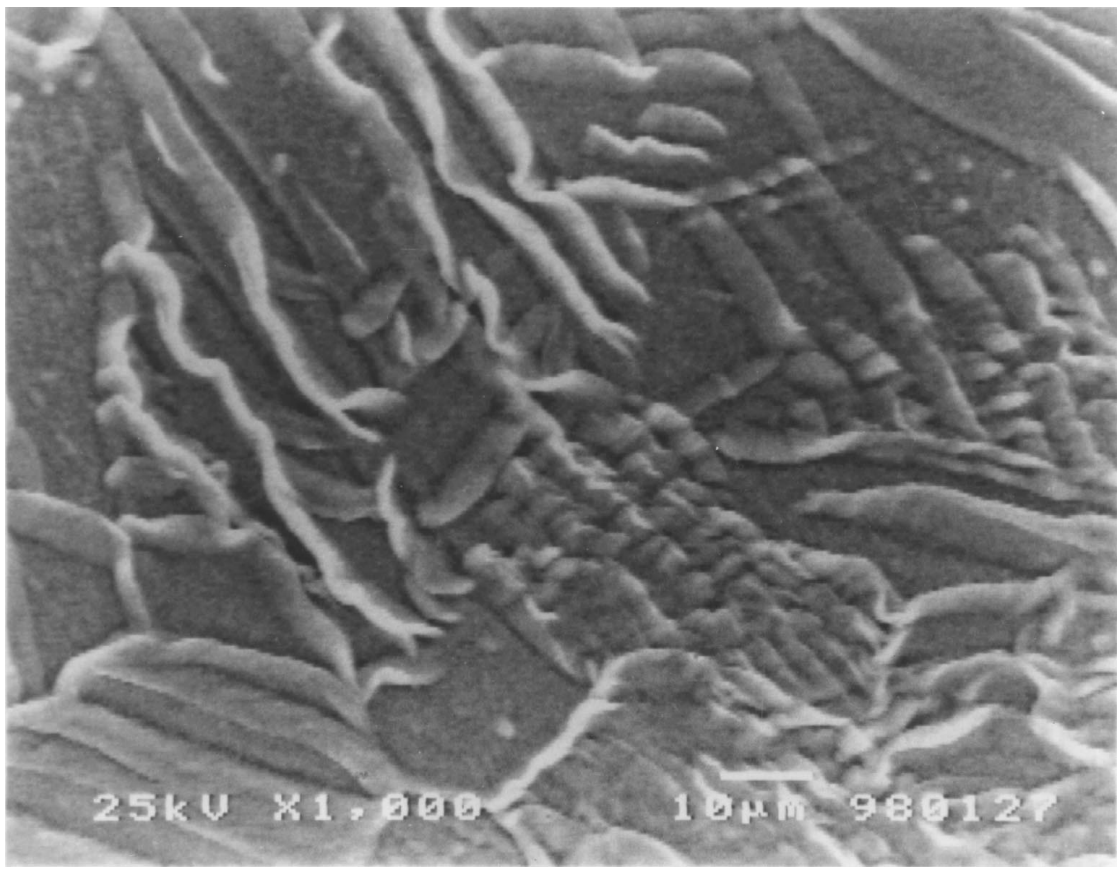

Figure 5 SEM micrograph of Ti implanted with 6.5×10^{20}, 9 MeV Au ions/m^2, showing accumulation of matter at the grain boundaries and on the grain surface.

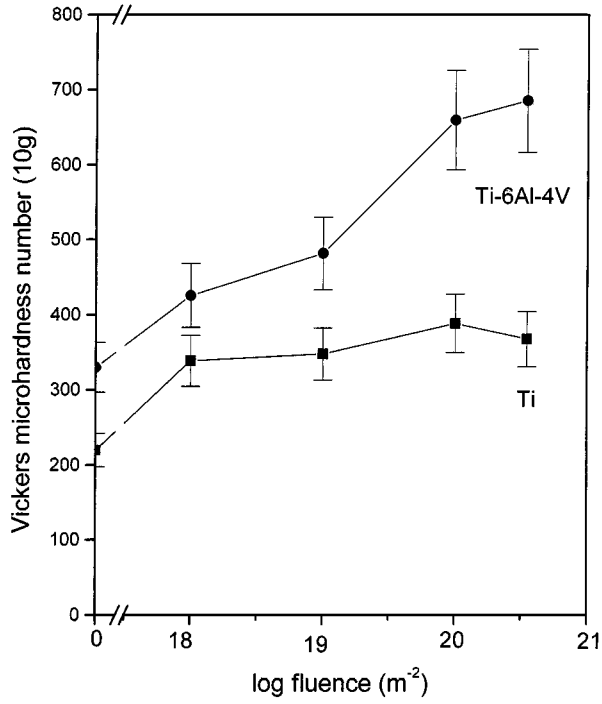

Figure 6 Dependence of Vickers microhardness measurements on Au ion fluence for Ti and Ti-6Al-4V samples.

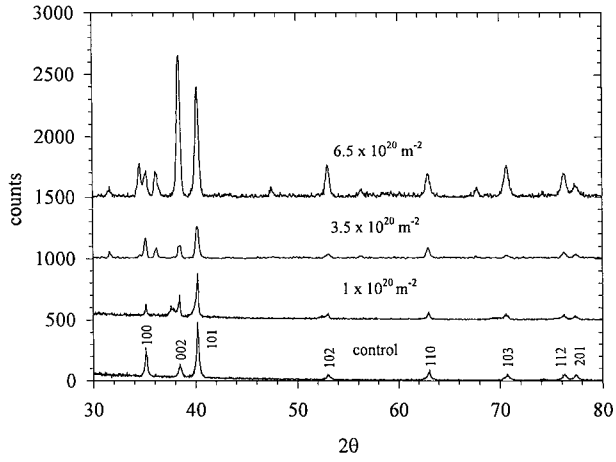

Figure 7 Comparison of diffraction patterns from a Ti reference sample and from samples implanted with 10^{20}, 3.5×10^{20}, and 6.5×10^{20} Au ions/m^2, with glancing angle $\alpha = 1^\circ$.

these cases the GXRD patterns taken at different values of grazing angle α showed no relevant change in the near-surface properties.

Fig. 7 shows a comparison of patterns from a reference sample and from samples implanted with 10^{20}, 3.5×10^{20}, and 6.5×10^{20} Au ions/m^2, with $\alpha = 1^\circ$. In the reference sample pattern the pure Ti lines are indicated. For a fluence of 10^{20} Au ions/m^2 there is evidence of a decrease in the lattice parameter a of 0.2% and an increase in c of 2%. As can be seen in the figure, the relative intensities of lines (100) and (002) were modified for the higher fluence, indicating that the implantation induced a change in crystal orientation.

In the samples with 3.5×10^{20} and 6.5×10^{20} Au ions/m^2 additional lines are observed. The sequence of new maxima can be explained as due to a new hcp structure with values of lattice parameters a and c of 0.3268 nm and 0.5184 nm, respectively, obtained from

TABLE I Indices of the new diffraction maxima observed in Ti and the alloy Ti-6Al-4V, at a fluence of 6.5×10^{20} Au ions/m^2, assuming an hcp structure

hkl	in Ti d(nm)	in Ti-6Al-4V d(nm)
100	0.2829	0.2803
002	0.2595	---
101	0.2484	0.2464
102	0.1912	0.1901
110	0.1630	0.1618
112	0.1381	0.1371
201	0.1364	0.1355

the measured values of interplanar distance d shown in Table I. Of the whole sequence pertaining to the new structure, the only maximum not observed (002) would be located underneath a strong peak (100) of the original structure. Both parameters a and c present an increase of approximately 10.7% with respect to the original Ti lines. The only line that does not belong to either of the hcp sequences is a weak one located at $2\theta = 43.54^\circ$, and coincides with the line of maximum intensity of the compound $AuTi_3$ [15]. The other reflections of this minority phase would be hidden in the background. There is the possibility that the new lines consistent with an hcp structure could be associated with an orthorhombic phase, but the corresponding parameters would be too large to be likely.

The analysis of the random microstrain and particle size broadening effect on the diffraction maxima of the original structure was performed by the Williamson-Hall plot method [16]. An example is shown in Fig. 8, which is a plot of $\beta \cos\theta$ vs. $\sin^2\theta/\beta\cos\theta$ for each of the successive diffraction maxima in a spectrum, where θ is the Bragg angle and β is the total width of each line. Only well resolved maxima were considered, and a straight line was fit to the experimental points. On the

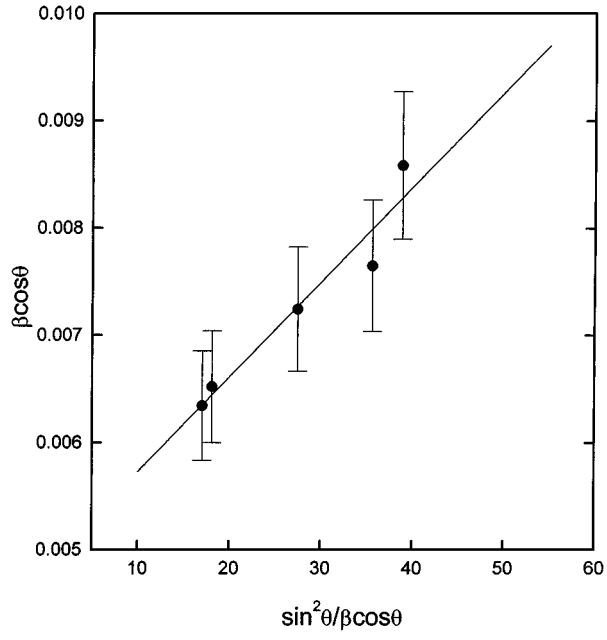

Figure 8 Example of a Williamson-Hall plot. The grain size is calculated from the intercept of the straight line with the vertical axis, and the rms value of the microstrain is obtained from the slope.

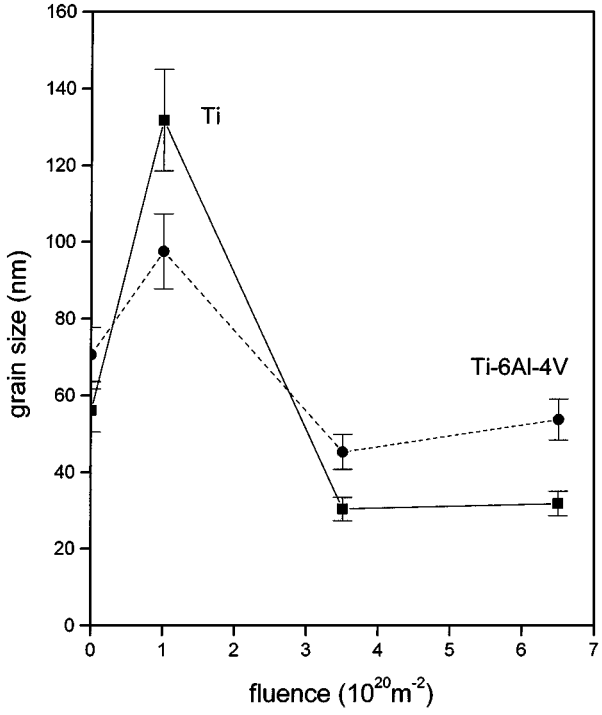

Figure 9 Values of grain size vs Au ion fluence, obtained from the Williamson-Hall plots corresponding to spectra of Ti and the Ti-6Al-4V alloy.

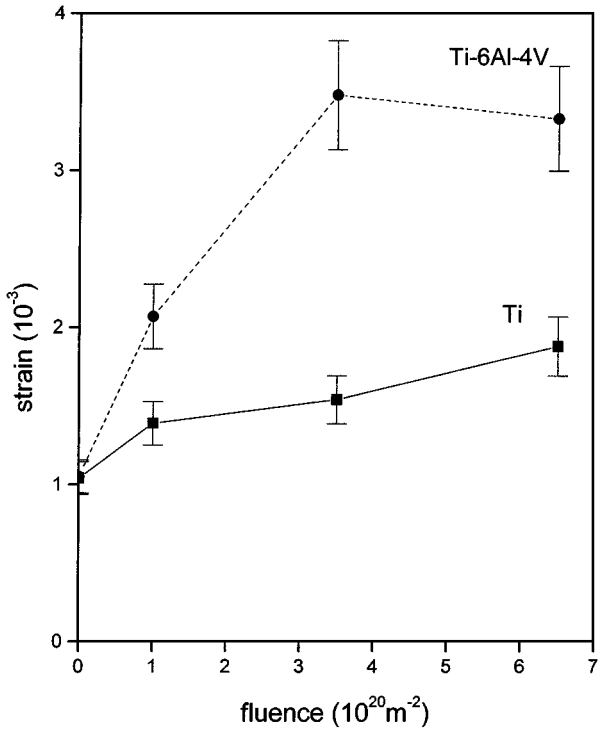

Figure 10 Values of microstrain vs Au ion fluence, obtained from the Williamson-Hall plots corresponding to spectra of Ti and the Ti-6Al-4V alloy.

plot, the grain size is calculated from the intercept of the straight line with the vertical axis, and the rms value of the microstrain is obtained from the slope. Plots from each of the samples indicate that both the grain size and the root mean square (rms) value of microstrain increase with depth in the reference sample, while in the sample exposed to the fluence of 1×10^{20} m^{-2} only the grain size increases, though less markedly, and the microstrain decreases with depth.

The Williamson-Hall plots were obtained for the diffraction maxima of the original hcp structure of samples implanted with 1, 3.5 and 6.5×10^{20} Au ions/m^2. The results are shown in Figs 9 and 10. In the case of Ti, the grain size increases to more than twice the original value at 10^{20} Au ions/m^2, and at higher fluence it drops to less than the original value. The microstrain, on the other hand, increases monotonically with fluence, and does not exceed twice the original value.

3.2. The alloy Ti-6Al-4V

These same kinds of measurements were also performed on the alloy Ti-6Al-4V samples. Fig. 11 shows the corresponding diffraction patterns for the same values of fluence as the case of Ti (10^{20}, 3.5×10^{20}, and 6.5×10^{20} Au ions/m^2, with $\alpha = 1^\circ$). The reference sample diffraction patterns are in agreement with the known structure [13] of V-depleted α phase grains (hcp with $a = 0.2925$ nm and $c = 0.4670$ nm) in a V-enriched β phase matrix (bcc with $a = 0.3230$ nm).

Four lines (110, 200, 211 and 220), of which only one is visible in Fig. 11, but appear in other diffraction patterns, allow the identification of the β phase in the reference samples. These lines show a gradual shift in XRD patterns for fluence values of 10^{18}, 10^{19}, and 10^{20} Au ions/m^2, corresponding to a decrease in the lattice parameter a of 1.5% at 10^{20} Au ions/m^2. The same was observed in GXRD with a decrease in a of 1.2%. At the higher fluence of 6.5×10^{20} Au ions/m^2 these lines were either hidden by one of the stronger peaks or in the background.

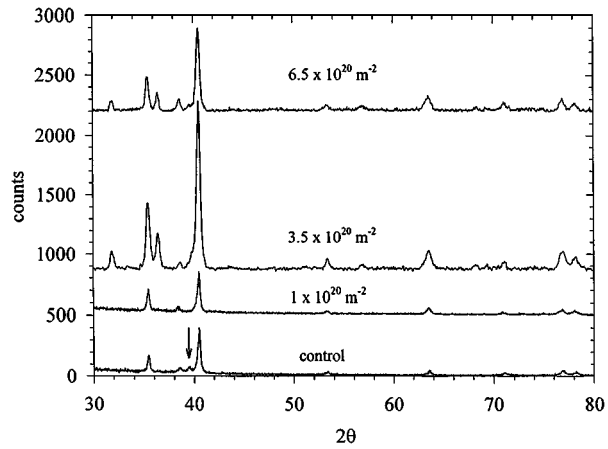

Figure 11 Glancing angle diffraction patterns from the Ti-6Al-4V alloy for reference samples and samples implanted with 10^{20}, 3.5×10^{20}, and 6.5×10^{20} Au ions/m^2, with $\alpha = 1^\circ$. The peak marked with an arrow is one of the bcc lines of the β phase; the other three are not visible in this spectrum.

At 3.5×10^{20} and 6.5×10^{20} Au ions/m^2 the same additional lines are observed as in the Ti case, corresponding to a new hcp structure with values of lattice parameters a and c of 0.3242 and 0.5168 nm, respectively, obtained from the measured values of d shown also in Table I. Again, both parameters present an increase of 10.7% with respect to the original Ti-6Al-4V lines. At the higher fluence, two lines were identified consistent with the $AuTi_3$ compound.

The grain size and microstrain were analyzed in the same way as the Ti samples, using Williamson-Hall plots. The results for the alloy are included in Figs 9 and 10. The changes in grain size show a behavior similar to the Ti case, but less marked. However, the microstrain increases with fluence to more than three times the original value, and then levels off. The accumulation of matter observed by SEM at grain boundaries and surfaces does not appear in the alloy samples.

4. Discussion

The RBS spectrum indicates that there was very little diffusion of the implanted Au. The maximum of the Au peak is within the error expected from the stopping powers employed by the computer codes used. The FWHM of the implanted Au, however, is larger than that expected from the TRIM calculation (0.62 μm vs 0.22 μm). This is not surprising, since the SEM micrographs show that the surface was strongly modified, and considerable roughness was introduced with the implantation.

Table II is a summary of the measured values of the lattice parameters a and c for the hcp structure (α phase) in reference Ti and Ti-6Al-4V, as well as Au ion implanted Ti and Ti-6Al-4V. The resulting ratio c/a is included for each case. In pure Ti, the implantation of Au leads to the appearance of the new phase with values of a and c 10.7% larger than the original Ti. In the Ti-6Al-4V alloy, the same is observed in the α phase: a new phase appears with values of a and c again 10.7% larger than the original alloy. In all cases the ratio c/a is very near 1.6, which is typical of the hcp structure. There is a resemblance of these structures with metastable phases obtained from ion mixing experiments leading to various alloys in which the major constituent originally has an hcp structure [17].

There is the possibility of the $AuTi_3$ phase being present, although only one peak is evident, that of maximum intensity, the (211) peak corresponding to a cubic structure. A TRIM calculation indicates that for the higher fluence (6.5×10^{20} Au ions/m^2) the Au concentration at the peak of the implanted Au is approximately 2.3 at. %. This is one tenth of the 25 at. % that corresponds to the $AuTi_3$ compound, so it is feasible that the compound exists in scattered precipitates. The conditions for a solid solution [18] of Au in Ti are not met: the atomic radii of the two elements are very different, the crystal structures are different, the values of electronegativity differ, and they have different valences. Therefore precipitates of $AuTi_3$ would be expected.

The calculated value of displacements per atom (dpa) is sufficiently large for amorphization to occur. However, not only does the original hcp structure persist, but at the higher values of fluence there is the advent of the new phase, in both the Ti and the Ti-6Al-4V alloy. This phase is formed mainly by structural damage produced by the beam, and not by the formation of compounds.

TABLE II Values of the lattice parameters a and c for the hcp structure (α phase) of reference Ti and Ti-6Al-4V, as well as Au ion implanted Ti and Ti-6Al-4V, measured in this experiment. The resulting ratio c/a is included for each case

	Reference	Implanted
Ti	$a = 0.2950$ nm	$a = 0.3268$ nm
	$c = 0.4686$ nm	$c = 0.5184$ nm
	$c/a = 1.588$	$c/a = 1.586$
Ti-6Al-4V	$a = 0.2925$ nm	$a = 0.3242$ nm
	$c = 0.4670$ nm	$c = 0.5168$ nm
	$c/a = 1.597$	$c/a = 1.594$

5. Conclusions

A study of the implantation of 9 MeV Au ions into Ti and the Ti-6Al-4V alloy has been made using various analytical techniques (RBS, XRD, GXRD, SEM). For both Ti and the Ti-6Al-4V alloy, at values of fluence above 10^{20} Au ions/m^2, structural damage leads to a new hcp phase, with larger values of lattice parameters a and c than the original material. In all the hcp phases observed (reference and implanted), the value of c/a is close to 1.6, which is typical of the hcp structure. There is also certain evidence of the formation of the $AuTi_3$ compound. No amorphization is evident in spite of large dpa values.

Acknowledgments

The authors wish to acknowledge the technical assistance of L. Baños (IIM-UNAM), K. López, J. Cañetas, L. Carapia (ININ), M. Galindo, and M. Guerrero. One of the authors (LRV) was supported by a scholarship from Dirección General de Estudios de Posgrado, U.N.A.M. The support of DGAPA-UNAM Project IN103995 and CONACYT Projects F036-E9109 and G0010-E is also acknowledged.

References

1. B. D. RATNER, A. S. HOFFMAN, F. J. SCHOEN and J. E. LEMONS (eds.), in "Biomaterials Science, An Introduction to Materials in Medicine" (Academic Press, 1996).
2. R. BOYER, G. WELSCH and E. W. COLLINGS (eds.), in "Titanium Alloys, Materials Properties Handbook" (ASM International, 1994).
3. M. J. DONACHIE JR., "Titanium: A Technical Guide" (ASM International, 1988).
4. P. SIOSHANSI and E. J. TOBIN, *Surface Coatings and Technology* **83** (1996) 175.
5. H. DAMMAK, A. BARBU, A. DUNLOP, D. LESUEUR and N. LORENZELLI, *Phil. Mag. Letters* **67** (1993) 253.
6. H. DAMMAK, A. DUNLOP and D. LESUEUR, *Phil. Mag. A* **79** (1999) 147.
7. R. BOYER, G. WELSCH and E. W. COLLINGS (eds.), in "Titanium Alloys, Materials Properties Handbook" (ASM International, 1994) p. 125.
8. *Idem., ibid.* (ASM International, 1994) p. 488.
9. J. F. ZIEGLER, J. P. BIERSACK and U. LITTMARK, "The Stopping and Range of Ions in Solids" (Pergamon Press, 1985).
10. W. K. CHU, J. W. MAYER and M. A. NICOLET, "Backscattering Spectrometry" (Academic Press, 1978).
11. L. R. DOOLITTLE, *Nucl. Instr. and Methods* **15** (1986) 227.
12. C. R. BROOKS, "Heat Treatment, Structure and Properties of Nonferrous Alloys" (American Society for Metals, Metals Park, Ohio, 1982) p. 332.

13. *Idem., ibid.* (American Society for Metals, Metals Park, Ohio, 1982) p. 369.
14. Powder Diffraction File 44-1294, ICDD, 1997.
15. Powder Diffraction File 18-578, ICDD, 1997.
16. G. K. WILLIAMSON and W. H. HALL, *Acta Metall.* **1** (1953) 22.
17. B. X. LIU, *Phys. Stat. Sol. (A)* **94** (1986) 11.
18. M. NASTASI, J. W. MAYER and J. K. HIRVONEN, "Ion-Solid Interactions: Fundamentals and Applications" (Cambridge University Press, 1996) p. 276.

Received 27 April 1999
and accepted 8 June 2000